A&A 389, 825–835 (2002)
DOI: 10.1051/0004-6361:20020680

Astronomy & Astrophysics

Star formation in the warped outer pseudoring of the spiral galaxy NGC 3642

L. Verdes–Montenegro[1], A. Bosma[2], and E. Athanassoula[2]

[1] Instituto de Astrofísica de Andalucía, CSIC, Apdo. 3004, 18080 Granada, Spain
[2] Observatoire de Marseille, 2 Place le Verrier, 13248 Marseille Cedex 4, France

Received 15 March 2002 / Accepted 26 April 2002

Abstract. NGC 3642 was classified as a spiral galaxy with three rings and no bar. We have performed an HI and optical study of this nearly face-on galaxy. We find that the nuclear ring might in fact be part of an inner one-armed spiral, that could be driving nuclear accretion and feeding the central activity in the inner kpc. The inner ring is faint, and the outer ring is a rather ill-defined pseudoring. Furthermore, the size ratio of the rings is such that they cannot be due to a single pattern speed linking them together. The outer pseudoring is peculiar, since it lies in the faint outer parts of the disk, where star formation is still going on at 1.4 times the optical radius. Higher HI column densities are associated with these regions and the atomic gas layer is warped. These perturbations affect only the outer disk, since the kinematics within the main body conforms well to an ordinary differentially rotating disk. We propose here that both nuclear activity and star formation in the warped outer parts might be linked to the fact that NGC 3642 is located in a rich environment, where its close neighbors show clear signs of merging. Our suggestion is that NGC 3642 has captured recently a low-mass, gas-rich dwarf, and star formation was triggered in this infalling external gas that produced also a pronounced warp in the gaseous disk.

Key words. galaxies: individual: NGC 3642 – galaxies: kinematics – galaxies: photometry – galaxies: spiral – galaxies: structure

1. Introduction

NGC 3642 was classified as unbarred (SAbc from RC3 – De Vaucouleurs et al. 1991, Sb(r)I from the RSA – Sandage & Tammann 1987) and has three rings (De Vaucouleurs & Buta 1980, hereafter DVB80). This combination was our main motivation for the study of this galaxy, as part of our analysis of ringed non-barred galaxies (Verdes-Montenegro et al. 1995, 1997, 2000). However, based on optical images, we have found that the outer ring is just a not very well defined pseudoring lying in the faint outer parts of the optical disk. Furthermore, when compared with the statistical study performed by Athanassoula et al. (1982) we find that the size ratio of the outer and inner ring is far larger than the one needed to link them to the ratio of a ring at the outer Lindblad radius and a ring near corotation due to a single pattern speed.

New HI data of this galaxy show that its outer disk is warped, and that star formation occurs beyond R_{25} (at $1.4 \times R_{25}$, where $R_{25} = 161'' \pm 3''$ from RC3). Star formation in the faint outer parts of galactic disks is a relevant and little understood issue: very few examples have been so far studied (Ferguson et al. 1998 and references therein). These combined characteristics make NGC 3642 an interesting galaxy, and in this paper we present a detailed optical and HI (WSRT) study.

The systemic heliocentric radial velocity of this galaxy, obtained from our HI data (Sect. 2.3) is 1572 km s^{-1}, and corrected to the centroid of the Local Group is 1682 km s^{-1}. A Hubble constant of 75 km s^{-1} Mpc^{-1} gives a distance of 22.4 Mpc for NGC 3642.

2. Observations and data analysis

2.1. Photometry

We have analysed optical data of NGC 3642 in the B and R bands. Boroson (1981) has obtained photographic surface photometry of this galaxy in the B-band. We have supplemented Boroson's data with CCD surface photometry extracted from an R-band image obtained from the ING archive. This image was obtained on February 3, 1995

Send offprint requests to: L. Verdes–Montenegro,
e-mail: lourdes@iaa.es

at the INT telescope with a 1024×1024 pixel TEK1 CCD camera, each pixel being 24 μm in size and $0.58''$. The measured seeing is $1.''7$. Flatfielding was achieved by producing a superflatfield from the median of all obtained sky flats. Several fields of Landolt phometric standards were also retrieved from the ING archive, for the calibration of the R image. We find good agreement with the profile given by Boroson for the inner parts. For the outer parts some disagreement is found and we checked that this is not due to a bad sky subtraction of our R image.

We have also inspected the HST image published by Barth et al. (1998) with the $F547M$ (V band) filter, which we retrieved from the archive. This image does not extend with sufficient signal to noise ratio to the inner ring but is well suited to explore the central part of NGC 3642, including the nuclear structure.

2.2. Radio observations

We have observed NGC 3642 in the 21 cm line of HI with the Westerbork Synthesis Radio Telescope (WSRT[1]) in 1983. We used 40 interferometers with spacings ranging from 36 m to 2844 m in steps of 72 m. This results in a synthesized beam of $13.''0 \times 15.''1$ ($\alpha \times \delta$) and first grating response at $10' \times 12'$ ($\alpha \times \delta$). We used a digital backend (Bos et al. 1981) resulting in 31 channel maps at heliocentric velocities 1463.3 to 1710.7 km s^{-1}. Hanning smoothing was applied on–line, giving a velocity resolution of twice the channel spacing of 8.2 km s^{-1}.

The data were edited and calibrated as explained in Verdes-Montenegro et al. (1995). A rms noise level of $\sim$1.13 mJy/beam was achieved after 12 hours of integration. In order to get a higher signal–to–noise ratio in the integrated HI distribution and associated radial velocity field, we convolved the map data with a Gaussian, leading to a beam size of $21.''4 \times 18.''4$ ($\alpha \times \delta$). Primary beam corrections have been applied to our maps.

The total HI emission in this galaxy was measured to be 66.16 ± 5.98 Jy km s^{-1} by Haynes & Giovanelli (1991) with the Green Bank radiotelescope and corrected for source to beam extent to 83.84 Jy km s^{-1}. The HI spectrum obtained by integrating the flux density in each channel map over an area containing the line emission is shown in Fig. 1, and the derived total flux is 44 Jy km s^{-1}. Hence we are missing emission, and comparison with the single dish spectrum indicates that it comes from those velocities where the emission is more extended (velocity range 1545–1590 km s^{-1}, see Sect. 3.2). From our spectrum we derive a systemic velocity, obtained as the mean velocity at 20% of the peak, of 1572 km s^{-1}. The spectrum has a $FWHM$ at the 20% level of 74 km s^{-1}.

[1] The Westerbork Synthesis Radio Telescope is operated by the Netherlands Foundation for Radio Astronomy with financial support from the Netherlands Foundation for the Advancement of Pure Research (N. W. O.).

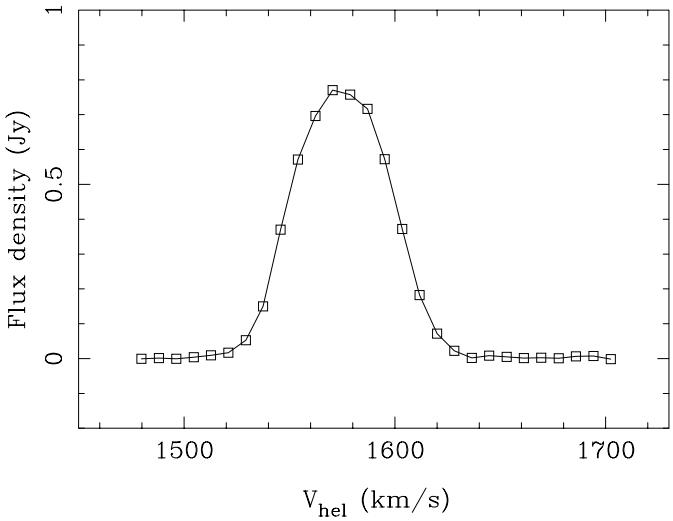

Fig. 1. HI flux density of NGC 3642 as a function of the heliocentric velocity.

3. Results and discussion

3.1. Optical emission

In Fig. 2a we show the R band image of NGC 3642. The central parts have been saturated in order to show better the outer spiral structure, that extends up to $220''$. We have marked with an ellipse the outer ring size given by DVB80, $\sim 5' \times 4'$. We do not find a complete outer ring in our image, although part of the ellipse seems to coincide with the wide outer spiral structure, that extends from about 145° to 325°. It is not obvious whether the thinner structure that extends from about 90° to 145° at smaller radius is part of the wider structure, or whether it corresponds to an inner spiral.

Boroson (1981) described the galaxy as having "at first glance a large bulge and a very faint disk", but indicated that "after closer examination it turns that much of the bulge region shows spiral structure, and is actually a section of the disk with a shorter scalelength". This (flocculent) spiral structure is shown in Fig. 2b, extending between radius $20''$ and $50''$, where the faint outer disk starts.

The spiral structure of NGC 3642 has a larger contrast in the outer parts than in the inner parts, and the difference between the two parts is more evident after substraction of a smoothed R image from the original one, that enhances the small scale structure (Fig. 2c). DVB80 reported the existence of an inner ring with a size of $25.''8 \times 22.''8$. This ring is faint in our R band image, and enhancement with unsharp masks is required in order to isolate it (Fig. 2d). We have measured its size as $28.''6 \times 25.''4$, in good agreement with DVB80, and its position angle as 0°.

The third ring reported by DVB80, a nuclear one with a diameter of $6''$, cannot be resolved in our R band image, where the central part is saturated due to the bright LINER nucleus (Heckman 1980). The inner $20''$ of NGC 3642 have bright emission in the HST-V image, that

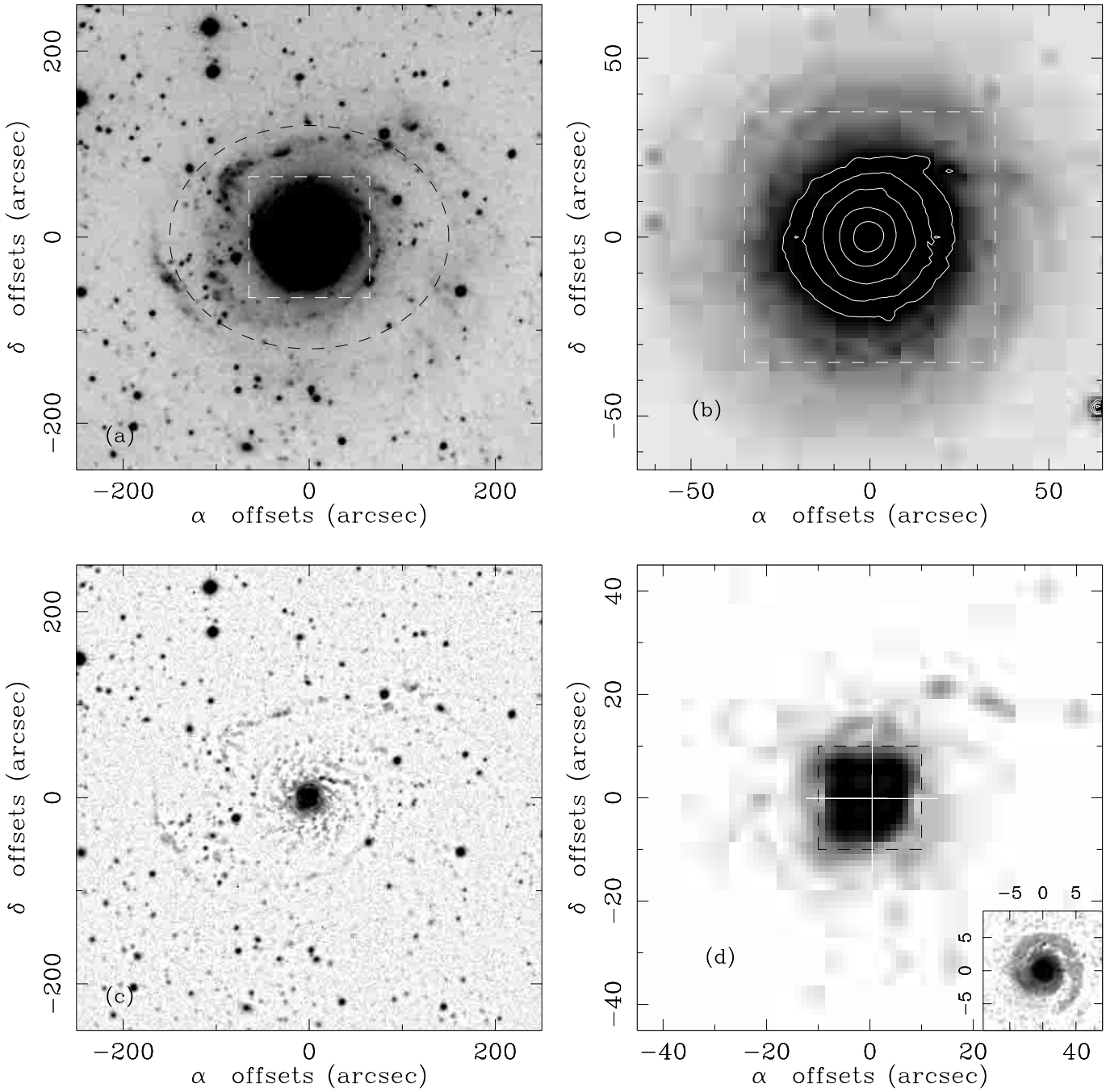

Fig. 2. a) R band image of NGC 3642 in a grey scale selected to show the outer spiral structure. The dashed box indicates the area shown in panel **b)**. The ellipse corresponds to the outer ring size given by DVB80, $\sim 5' \times 4'$. **b)** The same R image as in **a)** where the central area of the galaxy is shown. Isophotes at 19.6, 19.4, 19.1, 18.8, 18,6, 18.1 and 17.8 mag/arcsec^2 are plotted also. The dashed box indicates the area shown in panel **d)**. **c)** Sharpening of the R image obtained by the subtraction of a $9'' \times 9''$ box median filtered image. Darker areas correspond to excess emission. **d)** Close-up of the sharpened image shown in **c)** where the inner ring can be seen. The major and minor axe of the inner ring are marked. In the lower left inset we show the central part of the HST-V image (Sect. 2.1) , sharpened in order to show the single arm structure. It has been obtained by the subtraction of a $7'' \times 7''$ box median filtered image from the original one. Darker areas correspond to excess emission. The orientation of all the images is North up and East to the left, and the x and y axe are plotted as offset with respect to the optical center of the galaxy (Table 1).

shows sections (three quarters of a circle) of what could be the nuclear ring, with a diameter of $5''$. However a sharpening of the HST-V image (Fig. 2d) suggests that instead of a ring this emission enhancement is part of the nuclear spiral structure, since a single $m = 1$ spiral is observed, reaching the active nucleus, and extending between $1''$ and $6''$ from the center (109 to 654 pc at 22.4 Mpc), with several dust lanes crossing the outer part of the minispiral.

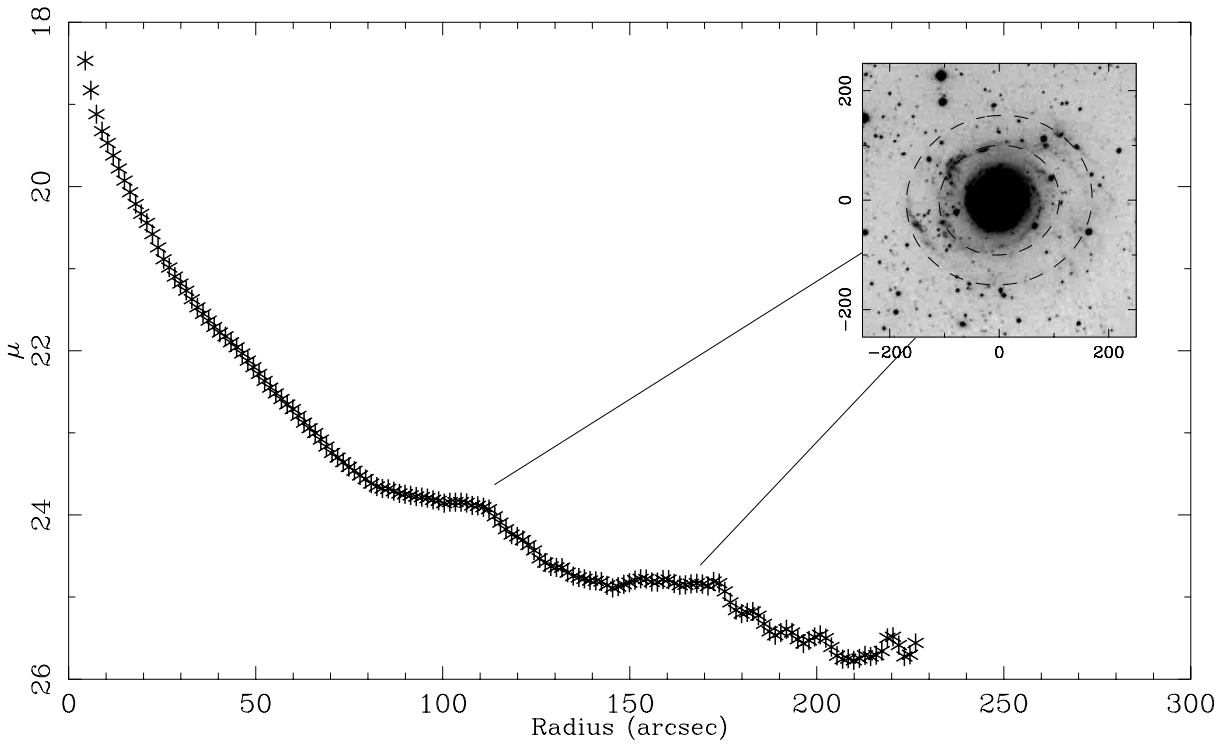

Fig. 3. R band radial brightness profile calculated by integrating the deprojected image over annuli circular in the plane of the galaxy, and with thickness of 1.″5, after star subtraction. The upper right inlay shows the location on the image of the areas corresponding to the bumps in the profile at radius 110″ and 170″.

At larger radii the arm seems to enter the flocculent structure that we have indicated above.

Hence NGC 3642 exhibits three different types of spiral structure: a nuclear one-armed minispiral, an inner flocculent spiral and an outer spiral that winds into an outer pseudoring extending for about half a circle. The winding direction of all three is the same (clockwise).

The radial brightness profile shown in Fig. 3 has been calculated from the R band by integrating over circular annuli with thickness of 1.″5 on the deprojected image of the galaxy (see Table 1 for the deprojection parameters), after blotting of the stars that project on the galaxy. Two bumps are evident on the profile at radii of 110″ and 170″, respectively, both associated with bright features in the spiral structure, as indicated in the upper right inlay. It is not surprising that such features appear in the R band since it includes the Hα line.

Ellipticities (ϵ) and position angles (pa) of the ellipses fitted to the R band isophotes are shown in Figs. 4a and b respectively as a function of radius, up to the larger radius at which we were able to perform such fitting (radius of 70″). The results are very noisy since the isophotes are strongly influenced by the spiral arms. The ellipticity shows a mean value of 0.06 ± 0.02, corresponding to an inclination of $i = 20.4° \pm 3.5°$, and the position angle does not show particularly abrupt changes with radius as expected for a bar embedded in a disk. There is also no obvious difference of the value of the inclination as function of radius, although the inner parts seem a bit more circular. Furthermore, there are no clearly marked minima in the light distribution corresponding to the Lagrangian points L_4 and L_5, a characteristic of the morphology of an oval distortion, nor is there any other sign of the presence of a bar. The low inclination makes the morphological determination of the position angle highly uncertain. Inside the inner pseudoring ($r < 14''$) the pa ranges between 125° and 160°. From 14″ to 20″, i.e. up to the beginning of the spiral structure, the p.a. drops steeply from 180° down to 110°. Then it jumps up to $\sim 158° \pm 44°$, between 20″and 70″.

3.2. Atomic gas distribution and kinematics

In Fig. 5 we display the channel maps containing the HI emission at the indicated heliocentric velocities, produced with a beam of 21.″4 × 18.″4. Each channel has a width of 8.2 km s^{-1} and an rms noise of 1.9 K, implying a level of 3.4×10^{19} cm^{-2}. The HI contours have been superimposed on the R-band image. There is a good correspondence between the brighter areas of HI emission and the outer spiral structure, as is also seen in the integrated HI map (Fig. 6). The brighest HI/optical features have column densities of 2.7×10^{21} cm^{-2}. At a level of 1.5×10^{20} cm^{-2} the galaxy extends ∼240″ in radius ($1.5 \times R_{25}$), offcentered by ∼25″ to the west. This is plausibly a lower limit to the real extent since we are missing nearly half of the flux (see Sect. 2.3). There is a central HI depression with N(HI) $\sim 1.0 \times 10^{19}$ cm^{-2}. The azimuthally averaged radial distribution of the HI column density is shown in Fig. 4c. It has been obtained by

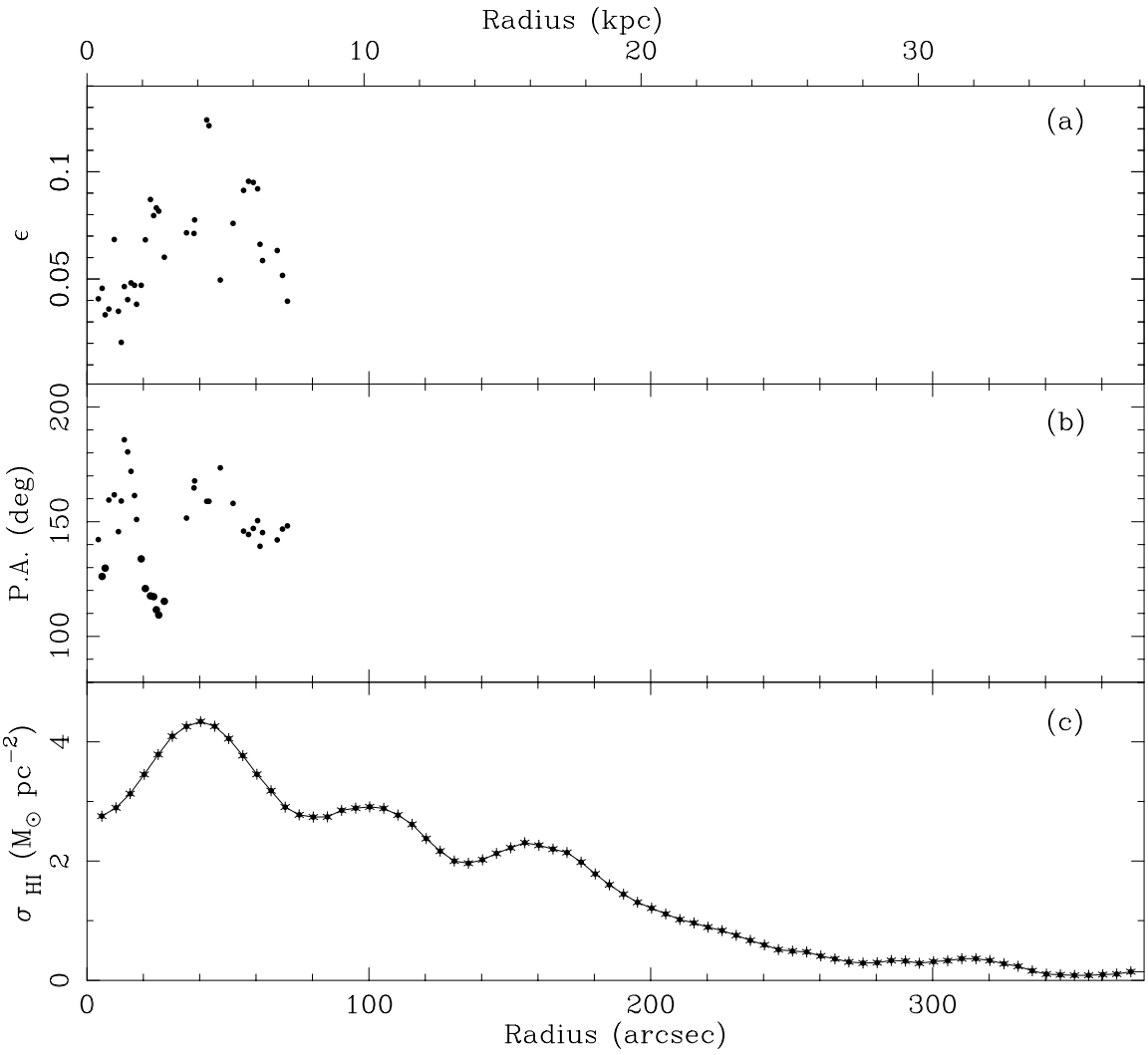

Fig. 4. Ellipticity **a)** and position angle **b)** of the ellipses fitted to the R band isophotes as a function of their semimajor axis length/radius (see Sect. 3.1). Angles are measured from N to E. **c)** HI surface density radial profile obtained as explained in Sect. 3.2. The lower radial scale is in arcsec and the upper one in kpc, for $D = 22.4$ Mpc.

averaging the two-dimensional HI distribution in elliptical rings using the geometrical parameters given in Table 1.

Numerous channel maps show emission at both receding and approaching sides of the galaxy. This results in the velocity field shown in Fig. 7a, where redshifted emission is observed in the blueshifted part of the velocity field and viceversa. Between 40″ and 70″ the isovelocity contours show kinks that correlate with the HI clumps associated to the spiral arms. But most of the perturbations for the largest radii are characteristic of a warped disk. We have derived the kinematical major axis based on the most symmetrical part of the velocity field ($r < 40''$). The major axis has been obtained as the direction perpendicular to the isovelocity contours, resulting in a value of pa = 122.6°. This direction coincides well with the line joining the peak of the blueshifted and redshifted velocities in the inner parts (Fig. 7). It differs significantly from the optically derived one, although this is not surprising due to the low inclination and the effect of the spiral structure on the isophotal fitting. We will thus adopt the pa of NGC 3642 derived from the velocity field. The isocontour at the systemic velocity (1572 km s^{-1}, Sect. 2.3) intersects the major axis direction at the optical center position, which we will also adopt as the kinematical center of the galaxy (Fig. 7b).

A cut along the major axis direction (Fig. 8, filled circles) shows clearly the radial velocity inversion observed in the velocity field. As we show in the next section, this can be modelled as a warped disk: due to the low inclination of the galaxy, any small difference in the inclination between the inner and outer parts can produce a large rotation of the major axis. We have overlapped the velocities obtained from a cut along the major axis of the velocity field. Declining velocities are observed for radii larger than 100″ down to values even lower than the systemic velocity.

3.3. Description of the warp model

We have modelled the velocity field fitting a tilted ring model (see Begeman 1987; the ROTCUR and GALMOD

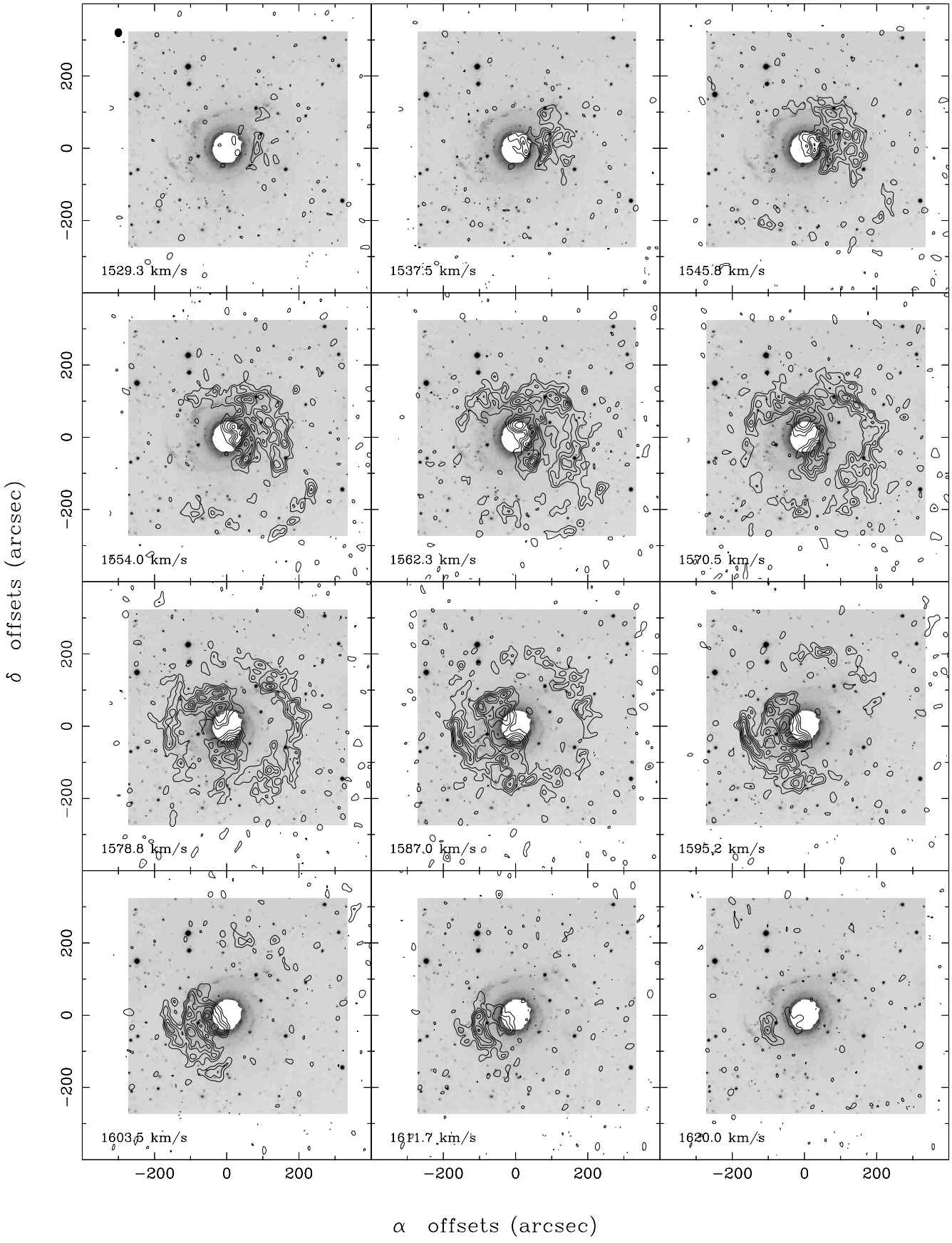

Fig. 5. Channel maps of the 21 cm line radiation superimposed on the R image, with the central part blotted for clarity. The heliocentric velocities are indicated in each panel. Contours correspond to 4.6, 7.6, 10.7, 13.7, 16.7 and 19.7 K, and the rms noise of the maps is 1.9 K. The synthesized beam ($21\farcs4 \times 18\farcs4 - \alpha \times \delta$) is plotted in the upper left panel.

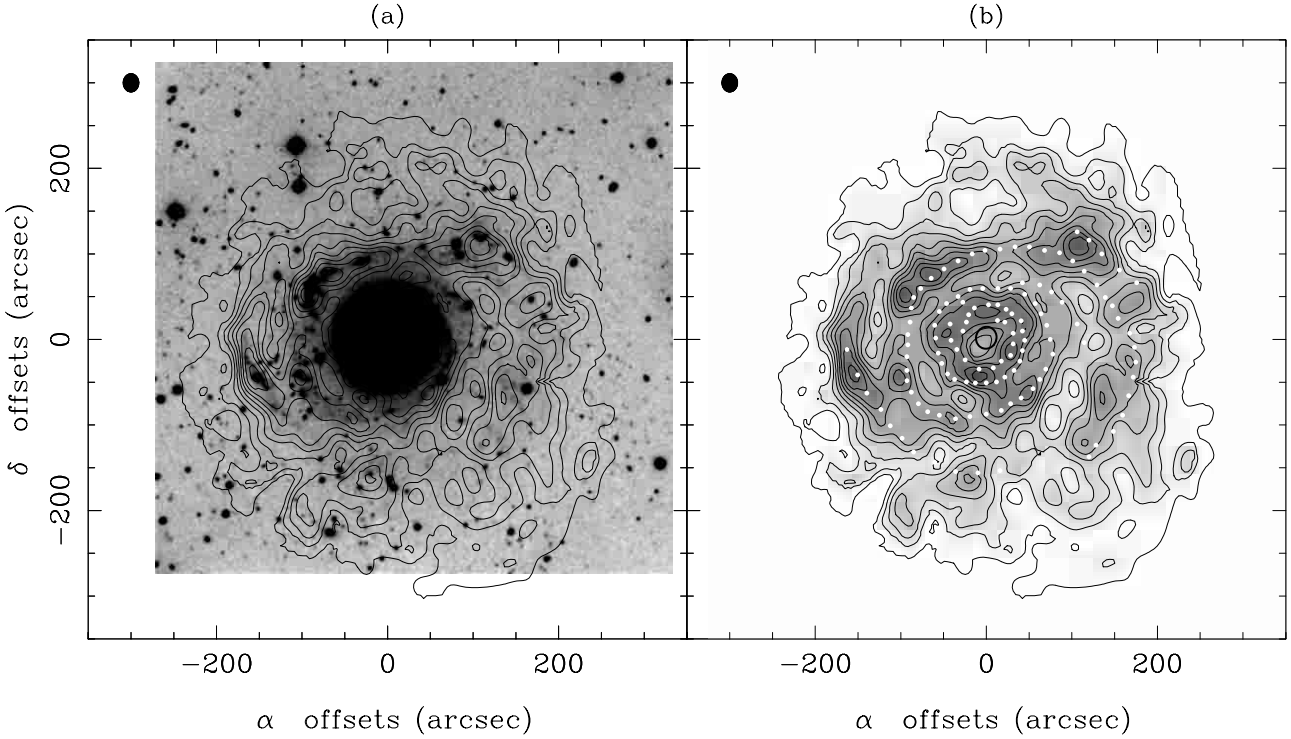

Fig. 6. a) Contour map of the HI column density distribution in NGC 3642 overlapped on the R image. The contours are 1.1, 3.4, 5.6, 7.9, 10.2, 12.4, 14.7, 16.9, 19.2 and 21.4×10^{20} atoms cm^{-2}. **b)** Greyscale map of the HI column density distribution with contours as in **a)**. The main features are marked as dots. The synthesized beam ($21\farcs4 \times 18\farcs4 - \alpha \times \delta$) is plotted in the upper left of both panels.

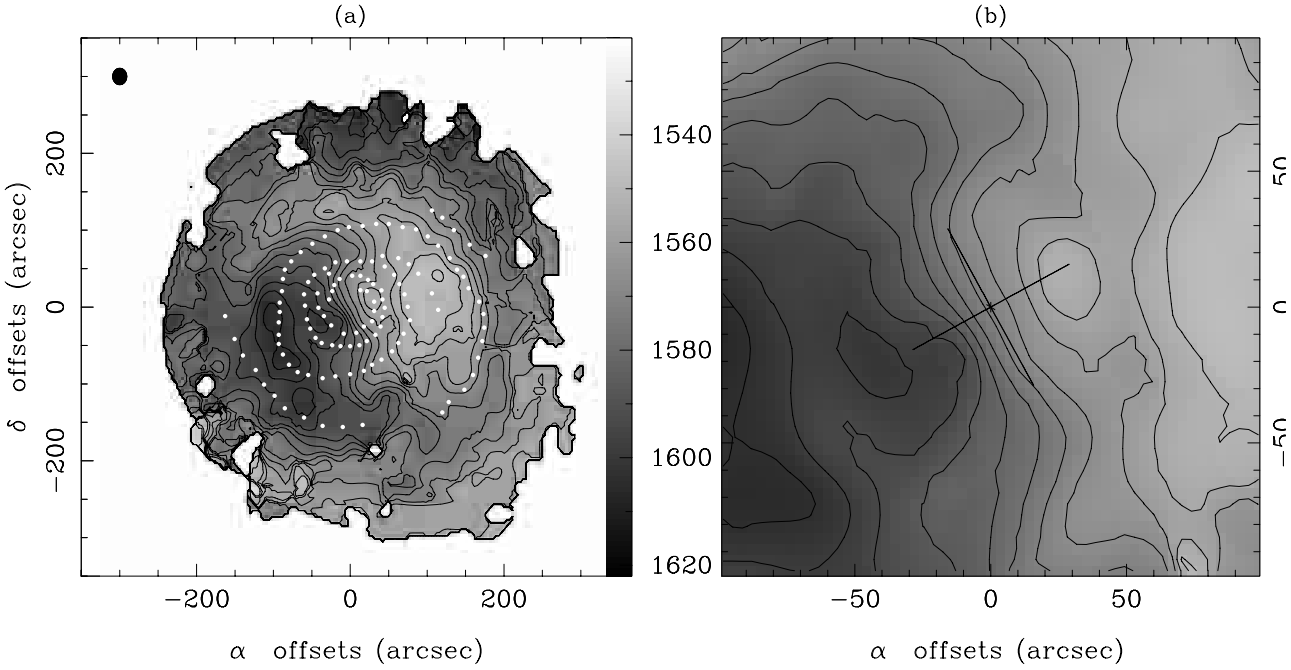

Fig. 7. a) Map of the first–order moment of the radial velocity field where both iso-velocity contours and greyscale are shown for clarity. The scale goes as in the wedge, where the numbers indicate heliocentric velocities in km s^{-1}. The contours go from 1532 to 1602 km s^{-1} with a step of 5 km s^{-1}. The main spiral features are marked as dots. The straight line indicates the direction of the position-velocity cut shown in Fig. 8. The beam size is $21\farcs4 \times 18\farcs4$ and is plotted in the upper left. **b)** Central part of the velocity field shown in **a)**. The major and minor axis directions are indicated, and a cross indicates the optical center position (see Sect. 3.2).

Table 1. Parameters of NGC 3642.

Center position[a]		
α(1950.0)		$11^{\rm h}\ 19^{\rm m}\ 25\overset{\rm s}{.}0$
δ(1950.0)		$59^\circ\ 20'\ 54\overset{''}{.}1$
Inclination (°)	adopted	$20.4^b \pm 3.5$,
	others	2^d, 34^e, 25^f,19^g
Position angle (°)	adopted	122.6^c
	others	$105^{d,e}$, 100^f
$B_{\rm T}{}^e$		11.65
$B^o_{\rm T}{}^e$		11.61
$R_{25}{}^e$		$161''$ (17.4 kpc)
HI systemic heliocentric velocity (km s^{-1})		1572^c,1588^e 1586^h

[a] Central position of NGC 3642 from Cotton et al. (1999).
[b] This paper, from ellipse fitting to the R band image.
[c] This paper from HI velocity field.
[d] UGC catalog.
[e] RC3.
[f] Boroson (1981).
[g] Kornreich et al. (1998).
[h] Haynes & Giovanelli (1991).

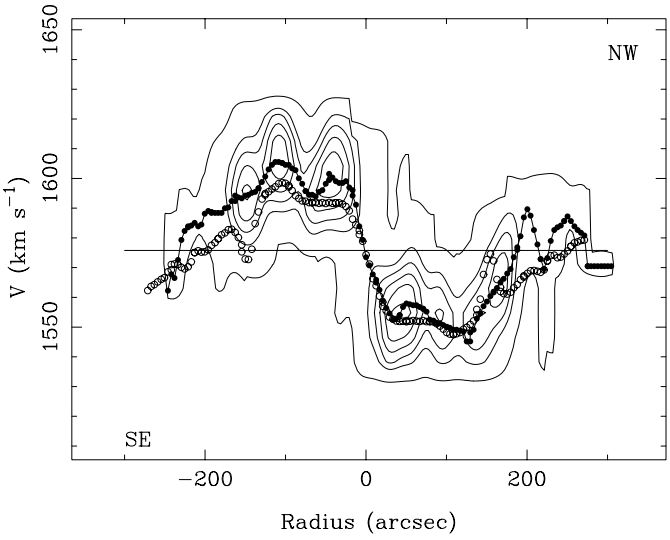

Fig. 8. Position-velocity diagram obtained across the major axis direction of the HI data cube. The plotted levels are 1.5, 6.1, 10.7, 15.2, 19.8, 24.4, 28.9, 33.5 and 38.1 K. Filled circles correspond to a cut along the observed velocity field (Fig. 7a), while the empty ones correspond to a cut along the modelled velocity field. The synthesized beam is $21\overset{''}{.}4 \times 18\overset{''}{.}4 - \alpha \times \delta$.

tasks in Gipsy). We have tried different combinations of the inclination, position angle and rotational velocity, as we describe below. In all cases the galaxy has been divided into concentric rings, each of them with a width of $5''$ along the major axis and a central position fixed to the optical center (Table 1). Points within a sector of 30° from the minor axis were excluded from the fits. The expansion velocities were set to zero and the systemic velocity fixed to the central velocity of the HI spectrum (Sect. 2.3, Table 1).

We could not allow the inclination and position angle to vary freely, since the errors for the inclination and for the rotation velocity are large for all radii. The galaxy is seen so face-on that a determination of the rotation curve is almost impossible: the uncertainties of the inclination correction are simply too large. Nevertheless, we have attempted to model the galaxy, assuming a flat rotation curve, as a continuation of what we find in the inner parts. From this we can estimate an approximate amplitude of the warping. In Fig. 9 we show the best combination of position angle and inclination that we have found in order to reproduce the velocity field. The inversion in the velocity field is reproduced although we could not obtain its most extreme features (Fig. 10). The fit along the major axis is however very accurate as shown in Fig. 8, where we compare the rotation curve along the major axis for the model and original data. The rotation curve, inclination and position angle obtained from our modelling are plotted in Fig. 9. The inclination derived from the modelling of the HI emission fits well with the one derived on the base of R band isophotal fitting. A warping of the disk of ∼25° is needed in order to reproduce the velocity field of NGC 3642. The bumps in the position angle at ∼90″ and 140″ coincide with the location of the spiral arms.

An estimate of the rotational velocity of this galaxy can be obtained from the Tully-Fisher relation (Pierce & Tully 1992). Using the observed M_B we get W_R = 379 km s^{-1}, which, combined with the observed extrema of the radial velocities, implies an inclination of 17°, in good agreement with our adopted value given the scatter in the Tully-Fisher relation.

3.4. Comment on the z-velocities in warps

The galaxies most useful for rotation curves studies are inclined typically between 50° and 80° (e.g. Begeman et al. 1991), and if a warp is present in the outer parts, its effect is traditionally modelled using a tilted ring model (Rogstad et al. 1974; Bosma 1978, 1981; Begeman 1987). Such a procedure, in particular the one implemented in ROTCUR, minimizes the importance of any peculiar motions, and maximizes the circular velocity in each ring independent of its spatial orientation. In reality, there ought to be some component of the motion of the inclined outer rings towards the main plane defined by the inner parts of the galaxy. We can get an upper limit to this motion by attributing to it all the peculiar motion seen in Fig. 8 (p-v-diagram along the major axis), which is 30 km s^{-1}. This can be compared to the rotation velocity, which is certainly larger than 80 km s^{-1}, and more likely of the order of 150 km s^{-1} or even 190 km s^{-1} (if the TF relation holds and the Sb(r)I classification of the RSA is retained). So at first order, z-motions of warps can be neglected.

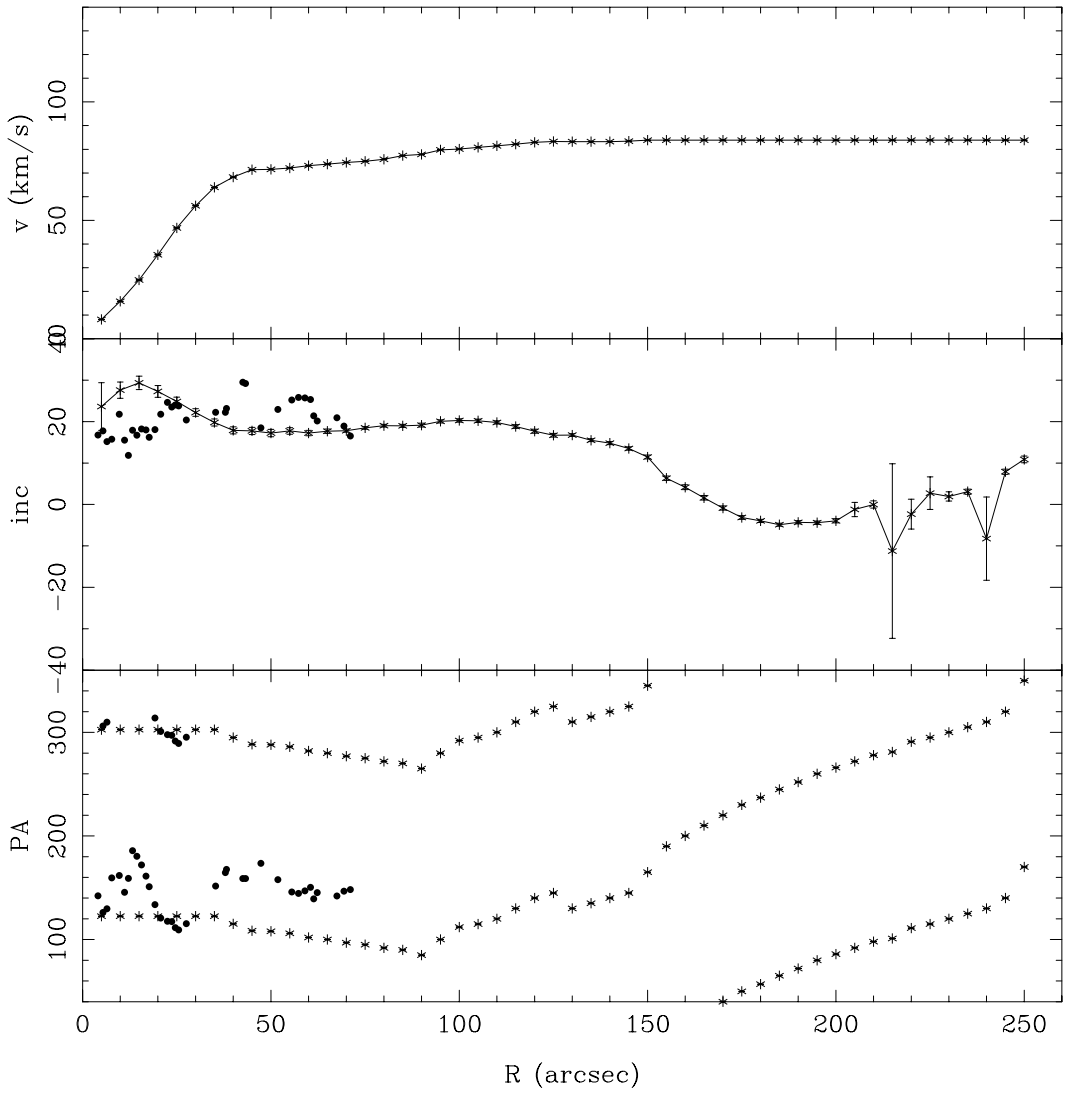

Fig. 9. a) Rotation curve assumed for the modelling of the velocity field. The best fit to this curve and to the observed velocity field is given by the combination of inclination and position angle plotted in **b)** and **c)** respectively. Filled dots correspond to the isophotal fitting of the optical R image (Fig. 4). Angles are measured from North to East.

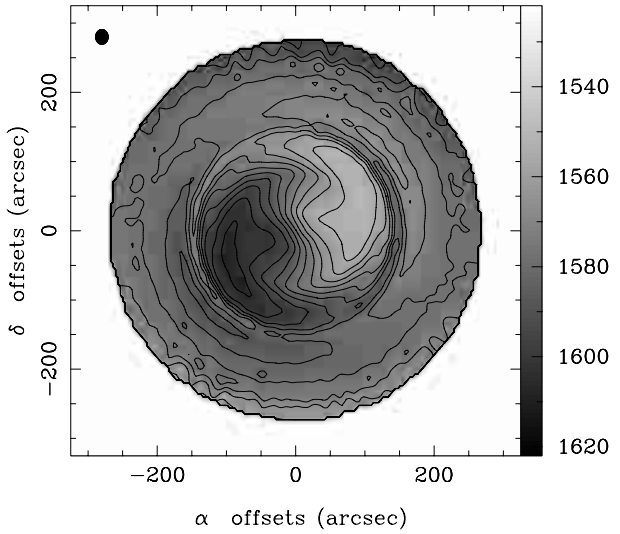

Fig. 10. First-order moment of the modeled channel maps obtained with the geometrical parameters plotted in Fig. 9.

Table 2. Derived parameters.

H I flux[a]	44 Jy km s^{-1}
H I flux[b]	84 Jy km s^{-1}
$M^a_{\rm HI}$	5.2×10^9 $M_\odot$
$M^b_{\rm HI}$	9.9×10^9 $M_\odot$
$M_{\rm HI}/L^0_B$	0.56

[a] This paper.
[b] Haynes & Giovanelli (1991).

3.5. Environment

We have studied the neighborhood of NGC 3642 within a radius of 500 kpc and 500 km s^{-1} and show the results in Fig. 11. From the NED[2] database we found that

[2] The NASA/IPAC extragalactic database (NED) is operated by the Jet Propulsion Laboratory, California Institute of Technology, under contract with the National Aeronautics and Space Administration.

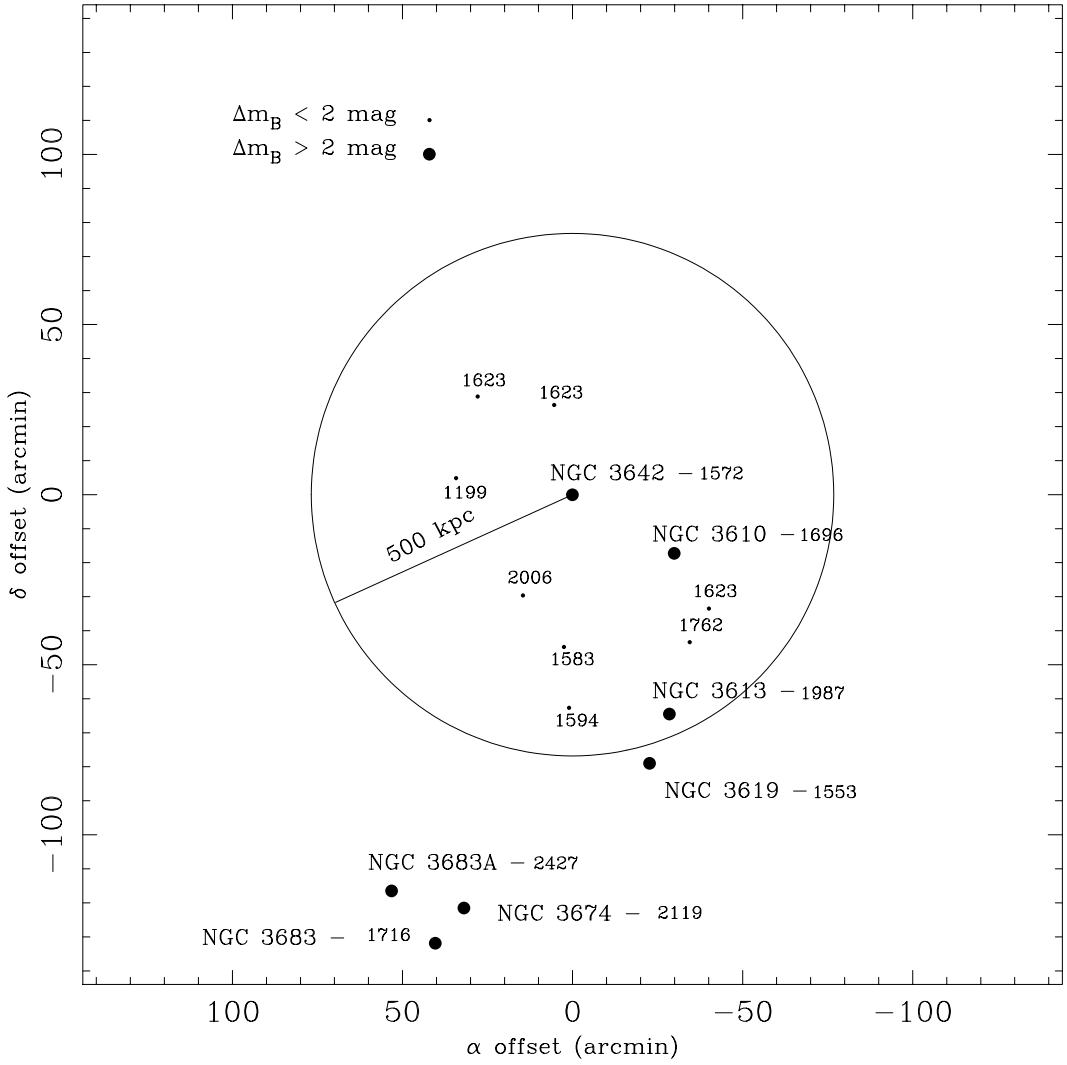

Fig. 11. The environment of NGC 3642. The circle encloses an area of 500 kpc radius centered on the galaxy. Those galaxies with a difference in blue magnitude less than 2 mag with respect to NGC 3642 are marked with larger circles, while the rest are marked with smaller ones. The velocities are also indicated.

NGC 3642 has 10 neighbors with known redshift in the box under consideration. Among them, NGC 3610 and NGC 3613 have magnitudes similar to that of NGC 3642, while the rest are fainter by more than 2 magnitudes. The closest companion, NGC 3610, is located at an apparent separation of 34′.7, or 226 kpc, and has clear signs of merger: this is a quite perturbed elliptical galaxy, with a prominent, edge-on stellar disk along the major axis in the inner regions (Scorza & Bender 1990). It has several shells, plumes and boxy outer isophotes indicating a past merger involving two disk galaxies dated 4 Gyr ago (cf. Whitmore et al. 1997) based on UBV colors. NGC 3613 is a disky elliptical with the disk fully embedded in a spheroidal component (Michard & Marchal 1994).

Garcia (1993) considered a larger scale, and finds that NGC 3642 belongs to a group composed by 5 galaxies. The brightest members of this group are NGC 3642 and 3610, followed by NGC 3619, a magnitude fainter, and by NGC 3674 and NGC 3683, which are two magnitudes fainter. The second nearby companion of NGC 3642 in mass, NGC 3619, is an early type disk galaxy with shells (cf. Schweizer & Seitzer 1988; Van Driel et al. 1989). The velocity dispersion of the group is 600 km s^{-1}. NGC 3683a is close to the group, although with a larger redshift (see Fig. 11).

4. Discussion and conclusions

We have investigated the optical morphology as well as the gas distribution and kinematics of the nearly face-on spiral galaxy NGC 3642. As is typical for spiral galaxies, the HI gas extends a factor of 1.5 beyond the optical radius. What is more unusual is that the outer HI regions composing the pseudoring are warped. Furthermore the HI is more extended in the western side, where the more external star forming area is located, and higher column densities are associated to these regions. These perturbations affect only to the outer disk, since the kinematics within

the main body conforms well to an ordinary differentially rotating disk.

The inner kpc of NGC 3642 shows a one-armed spiral structure. Spirals in the inner kpc of active galaxies have been considered as drivers of accretion into the central engine (Regan & Mulchaey 1999). While barred galaxies tend to show bisymmetrical patterns (Athanassoula 1992) non barred ones can have more irregular structures. The observed spiral could be driving nuclear accretion.

Both phenomena, nuclear activity and star forming warped outer parts, might be linked to the fact that NGC 3642 is located in a rich environment. Given the clear signs of merging in its closest bright companions, it is reasonable to assume that NGC 3642 also underwent recently an interaction, or, more likely, captured a low-mass, gas-rich dwarf, which disintegrated, and whose debris now form the outer HI and the outer patchy spiral structure in NGC 3642 itself. The differences in the kinematics between the approaching and receding sides of the galaxy are probably due to the accretion of a companion. The low surface brightness extension of the galaxy, as seen in the photometric structure, also points in this direction. Such low surface brightness extensions have been studied before, (e.g. Longmore et al. 1979; Bosma & Freeman 1993), and are not so uncommon. Longmore et al. (1979) indicated already that under favorable initial conditions, specially a low relative velocity encounter, a considerable fraction of the gas content of a galaxy can be drawn out in an interaction, and yet participate in subsequent star formation. We could therefore see star formation in the denser regions of redistributed material. i.e. in the outer pseudoring, which might be in the process of forming a continuous ring.

In conclusion, the observed outer and perhaps even the nuclear structure of the unbarred galaxy NGC 3642 can be attributed to accretion of an HI-rich dwarf galaxy that could be acquired from its rich environment. Star formation was triggered in its outskirts by incorporation of external gas that produced also a pronounced warp in the gaseous disk. Our modeling of the velocity field of this face-on galaxy allowed us to set a constrain on the amplitude of the z-motions in warps, which we find to be smaller than about 30 km s^{-1}. It could well be that the formation of some of the faint outer extensions of galactic disks is due to this kind of destruction of a low-mass, gas-rich dwarf during capture.

Acknowledgements. LV–M acknowledges the hospitality and financial support of the Observatoire de Marseille, where part of this work was carried out. LV–M is partially supported by AYA 2000-1564 and Junta de Andalucía (Spain).

References

Athanassoula, E., Bosma, A., Crézé, M., & Schwarz, M. P. 1982, A&A, 107, 101
Athanassoula, E. 1992, MNRAS, 259, 345
Barth, A. J., Ho, L. C., Filippenko, A. V., & Sargent, W. L. W. 1998, ApJ, 496, 133
Begeman, K. 1987, Ph.D. Thesis, University of Groningen
Begeman, K. G., Broeils, A. H., & Sanders, R. H. 1991, MNRAS, 249, 523
Boroson, T. 1981, ApJS, 46, 177
Bos, A., Raimond, E., & van Someren Greve, H. W. 1981, A&A, 98, 251
Bosma, A. 1978, Ph.D. Thesis, University of Groningen
Bosma, A. 1981, AJ, 86, 1825
Bosma, A., & Freeman, K. C. 1993, AJ, 106, 1394
Cotton, W. D., Condon, J. J., & Arbizzani, E. 1999, ApJSS, 125, 409
De Vaucouleurs, G., & Buta, R. 1980, AJ, 85, 637 (DVB80)
De Vaucouleurs, G., De Vaucouleurs, A., Corwin, H. G., et al. 1991, Third Reference Catalogue of Bright Galaxies (Springer, Berlin)
Ferguson, A. M. N., Wyse, R. F. G., Gallagher, J. S., & Hunter, D. A. 1998, ApJ, 506, L19
Garcia, A. M. 1993, A&AS, 100, 47
Haynes, M. P., & Giovanelli, R. 1991, ApJS, 77, 331
Heckman, T. M. 1980, A&A, 87, 152
Kornreich, D. A., Haynes, M. P., & Lovelace, R. V. E. 1998, AJ, 116, 2154
Longmore, A. J., Hawarden, T. G., Cannon, R. D., et al. 1979, MNRAS, 188, 285
Michard, R., & Marchal, J. 1994, A&AS, 105, 481
Pierce, M. J., & Tully, R. B. 1992, ApJ, 387, 47
Regan, M. W., & Mulchaey, J. S. 1999, AJ, 117, 2676
Rogstad, D. H., Lockart, I. A., & Wright, M. C. H. ApJ, 193, 309
Sandage, A., & Tammann, G. A. 1987, A revised Shapley-Ames Catalog of Bright Galaxies (Carnegie Inst. of Washington, Publ.), 635
Schwarz, M. P. 1985, MNRAS, 212, 677
Scorza, C., & Bender, R. 1990, A&A, 235, 49
Staveley–Smith, L., & Davies, R. D. 1987, MNRAS, 224, 953
Verdes–Montenegro, L., Bosma, A., & Athanassoula, E. 1995, A&A, 300, 65
Verdes–Montenegro, L., Bosma, A., & Athanassoula, E. 1997, A&A, 321, 754
Verdes–Montenegro, L., Bosma, A., & Athanassoula, E. 2000, A&A, 359, L23
Whitmore, B. C., Miller, B. W., Schweizer, F., & Fall, S. M. 1997, AJ, 114, 1797